Henri Stephan

# Senior Design Project Portfolio

The following document is representative of the design and manufacturing work performed by Henri Stephan for the All Brakes No Gas senior design team for the SDSU FSAE race team.

## Table of Contents



## Table of Tables



## Table of Figures

## Table of Equations

## Section 1: Calculations performed to help estimate the power involved in regenerative braking.

These figures are to be used to define the overall efficiency of regenerative braking.

The following equation calculates the total power required to slow the car from maximum velocity at maximum deceleration.

$$P_{braking} = \left( mg\mu_r + \frac{1}{2} C_D A\rho (V_{max} - V_{wind})^2 + m\delta \left(\frac{dV}{dt}\right)\right) V_{max} \tag{1}$$

Tables 1 and 2 outline the system parameters, defines variables from Equation 1, and tabulate the power calculations of the system.

*Table 1: System Parameters*

| System Parameter | Value | System Parameter | Value | System Parameter | Value |
|---|---|---|---|---|---|
| Mass (car + driver) (m) | 295 kg | Delta ($\delta$) | 1.04 | Density of Air ($\rho$) | 1.17 kg/$m^3$ |
| Drag Coefficient($C_D$) | 0.3 | Rolling Friction Coefficient ($\mu_r$) | 0.01 | Maximum Braking Deceleration$\left(\frac{dV}{dt}\right)$ | -10.79 m/$s^2$ |
| Cross-Sectional Area (A) | 0.56 $m^2$ | Velocity Max ($V_{max}$) | 24 m/s | Wind Velocity ($V_{wind}$) | 0 m/$s^2$ |

*Table 2: Power Calculation Results*

| Power Calculations | | | | | | | |
|---|---|---|---|---|---|---|---|
| Maximum Power from Braking | | | 78 kW | | | | |
| Power through Emrax during Generation (kW) | | Available Continuous Power (ACP) (kW) | | Avg ACP (kW) | | Power to Flywheel (kW) | |
| Best of Best (BOB) $\eta = 0.98$ | 76.5 | BOB | 46.1 | BOB | 30.7 | BOB | 24.9 |
| Worst of Worst (WOW) $\eta = 0.5$ | 39 | WOW | 23.5 | WOW | 15.7 | WOW | 12.7 |

As the regenerative brakes were meant to be integrated into the rear axle alone, further calculations were needed to define the required power for max braking force on just the rear wheels. This was done using a free body diagram to first develop an equation for the normal force on the rear tires. Equation 2 includes wheelbase (*l* in m), distance from rear axle to center of gravity ($a_2$ in m), height of center of gravity (*h* in m) acceleration (*a* in $\frac{m}{s^2}$), mass (*m* in kg), and the acceleration of gravity (*g* in $\frac{m}{s^2}$).

$$F_{z2} = \frac{1}{2} mg \frac{a_2}{l} + \frac{1}{2} mg \frac{ha}{lg} \tag{2}$$

Following this calculation, the horizontal force decelerating the car can be calculated using $F_{Z2}$ and the coefficient of static friction, which for the AER car's tires is 1.5. Multiplying the horizontal force by the tire radius ($r$ = 0.206 m) allows for calculation of the torque on the rear axle.

$$F_{X2} = \mu_s F_{Z2} \tag{3}$$

$$\tau_{axle} = F_{X2} r \tag{4}$$

The resulting torque on the rear axle can then be divided by the final drive ratio to find the torque at the output shaft. The torque at the output shaft can then be multiplied by the angular velocity at maximum output for the power generation in an ideal scenario. This method results in a power generation of 18.2 kW.

$$\tau_{motor} = \frac{\tau_{axle}}{Final\ Drive} \tag{5}$$

$$P = w\tau_{motor} \tag{6}$$

Table 3 outlines the resulting power calculations to determine the power to the flywheel.

*Table 3:Vehicle Dynamics Power Calculations*

| Power Calculations | | | | | | | |
|---|---|---|---|---|---|---|---|
| Maximum Power from Braking | | | 18.2 kW | | | | |
| Power through Emrax during Generation (kW) | | Available Continuous Power (ACP) (kW) | | Avg ACP (kW) | | Power to Flywheel (kW) | |
| Best of Best (BOB) $\eta = 0.98$ | 17.8 | BOB | 10.7 | BOB | 7.13 | BOB | 6.42 |
| Worst of Worst (WOW) $\eta = 0.5$ | 9.1 | WOW | 5.49 | WOW | 3.66 | WOW | 3.3 |

The following table illustrates the power required from the motor on the rear axle for various levels of deceleration. This assumes perfect efficiency and can be used as a baseline to determine actual efficiency of the system. This takes into consideration the forward weight transfer and as a result reduced traction on the rear axle as the vehicle decelerates more aggressively.

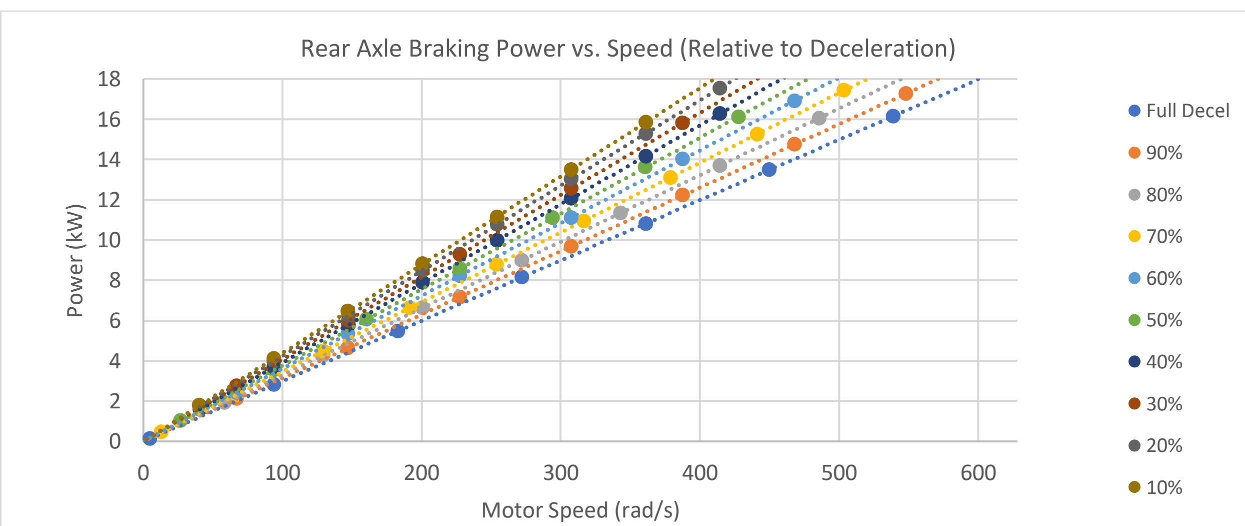


*Figure 1: Braking Power Analysis*

## Section 2: Flywheel Design and Calculations

Before the project was switched over to a more traditional regenerative braking system due to part lead times, budget, and a change in provided parts from AER; a flywheel energy storage system was proposed. The following trade study was performed to decide the material used in the flywheel.

*Table 4: Flywheel Material Trade Study*

| Design Criteria | Weight (%) | AISI 304 Steel | | | Ductile Iron | | |
|---|---|---|---|---|---|---|---|
| | | Rating (R) | Description | Weight Score (R x %) | Rating (R) | Description | Weight Score (R x %) |
| Yield Strength | 20 | 2 | 30,000 psi | 40 | 3 | 80,000 psi | 60 |
| Young's Modulus | 25 | 4 | 27,560 ksi | 100 | 2 | 17,400 ksi | 50 |
| Poisson's Ratio | 15 | 4 | 0.29 | 60 | 3 | 0.31 | 45 |
| Mass Density | 40 | 5 | $0.2890\ \frac{lb}{in^3}$ | 200 | 3 | $0.2565\ \frac{lb}{in^3}$ | 120 |
| Total | 100 | | | 400 | | | 275 |

The maximum vehicle velocity possible is $25.4\ \frac{m}{s}$; this was calculated using the final drive ratio of 5.1, the tire radius of 0.206 m, and the Emrax's max RPM of 6,000. The minimum velocity of the race was determined to be approximately $11.1\ \frac{m}{s}$ through existing velocity profiles. Using these velocities and the maximum possible deceleration of 1.1 g provided by the team's sponsor, it was determined that maximum regeneration could occur for 1.32 seconds. Taking into consideration the gradual application of the brakes, and the use of "trail braking" into the corner, this number was rounded down to 1.0 seconds. With this time frame, even in the worst-case scenario (Table 3), at least 3.3 kJ of storage would be required. Due to the magnitude of this value, the limiting factors for the dimensions of the flywheel will be the space, mass, and safety constraints set forth by the team. To store the maximum possible amount of energy with the minimum amount of mass possible, a design must be used that concentrates the most mass as far as possible from the axis of rotation of the flywheel. This can be seen in the formulas for the kinetic energy of a uniform disk (Equation 7) and a hollow cylinder (Equation 8), respectively. The equation accounts for mass (*m* in kg), radius (*R* in m), and angular velocity ($\omega$ in rad/s).

$$E = \frac{1}{4} mR^2 w^2 \tag{7}$$

$$E = \frac{1}{2} mR^2 w^2 \tag{8}$$

As a result, a rim design was chosen over a uniform disk design or truncated conical disk. The rim design remains within the team's defined safety parameters, while having superior energy storage and reduced mass.

*Table 4: Flywheel Shape Trade Study*

| Design Criteria | Weight (%) | Truncated Conical Disc | | | Rim with Spokes | | |
|---|---|---|---|---|---|---|---|
| | | Rating (R) | Description | Weight Score (R x %) | Rating | Description | Weight Score |
| Manufacturing Feasibility | 20 | 3 | The design tapers to the edge and contains fillets throughout that can be turned on a lathe. | 60 | 4 | There is no tapering to the design and the spokes can be milled. | 80 |
| Safety | 40 | 5 | Contains a FOS of 20. | 200 | 5 | Contains a FOS of 6. | 200 |
| Weight (with AISI 304 Steel) | 10 | 4 | 20.6 lbs | 40 | 3 | 17.8 lbs | 30 |
| Rotational Energy | 30 | 2 | Most of the weight is located centrally. | 60 | 5 | Most of the weight is located on the outer rim. | 150 |
| Total | 100 | | | 360 | | | 460 |

To determine the actual dimensions of the rim design, further calculations must be performed. Equation 8 allows for the calculation of the mass of the outer rim using the angular velocity of the auxiliary motor (3,000 – 3,500 RPM), the desired stored energy, and the desired outer radius of the rim. Then using the density of steel (8,000 $\frac{kg}{m^3}$), and the formula for the volume of a hollow cylinder, possible combinations of rim thickness ($r_1 - r_2$) and rim height ($h$) can be determined for the design (see Equation 9). This method was used to develop five preliminary designs, which could then be chosen from based on their safety, mass, and storage capacity. Design 5 was chosen because it has the highest kinetic energy storage (5.5 kJ), remains within the defined size constraints, and has a factor of safety of 8.7.

$$m = \rho \pi h (r_1^2 - r_2^2) \tag{9}$$

*Table 5: Preliminary Flywheel Dimensions*

| Prototype Design # | Mass (kg) | Outer Radius (mm) | Rim Thickness (mm) | Rim height (mm) | Rotational Velocity (RPM) | Factor of Safety | Energy Storage (kJ) |
|---|---|---|---|---|---|---|---|
| 1 | 5 | 111 | 31 | 33 | 3,000 | 7.07 | 3 |
| 2 | 5 | 111 | 61 | 20 | 3,000 | 6.74 | 3 |
| 3 | 8 | 87 | 39 | 60 | 3,000 | 17.5 | 3 |
| 4 | 8 | 111 | 45 | 40 | 3,000 | 11.8 | 5 |
| 5 | 8.8 | 101 | 40 | 42.5 | 3,500 | 8.7 | 5.5 |

Table 6 is based on the information in Table 7.

*Table 6: Flywheel Dimension Trade Study*

| Criteria | Weight % | 1 | | | 2 | | | 3 | | | 4 | | | 5 | | |
|---|---|---|---|---|---|---|---|---|---|---|---|---|---|---|---|---|
| | | Rating | Desc. | Score | Rating | Desc. | Score | Rating | Desc. | Score | Rating | Desc. | Score | Rating | Desc. | Score |
| Mass | 40 | 5 | 5 kg | 200 | 5 | 5 kg | 200 | 3 | 8 kg | 120 | 3 | 8 kg | 120 | 3 | 8.8 kg | 120 |
| F.S. | 20 | 3 | 7.1 | 60 | 3 | 6.7 | 60 | 5 | 17.5 | 100 | 4 | 11.8 | 80 | 3 | 8.7 | 60 |
| Energy Storage | 40 | 2 | 3 kJ | 80 | 2 | 3 kJ | 80 | 2 | 3 kJ | 80 | 4 | 5 kJ | 160 | 5 | 5.5 kJ | 200 |
| Total | 100 | | | 340 | | | 340 | | | 300 | | | 360 | | | 380 |

Further modifications were made to the proposed flywheel geometry to allow for a safer and more compact system. The following table uses the formulas in Equation 8 and Equation 9 in an Excel to model to determine the most efficient flywheel in terms of mass and energy storage. A line of efficiency was defined on the graph and all of the designs above said line were considered. The 4.19 kJ design was chosen as it was both well above the line of efficiency and had the highest energy storage capacity at 3500 RPM.

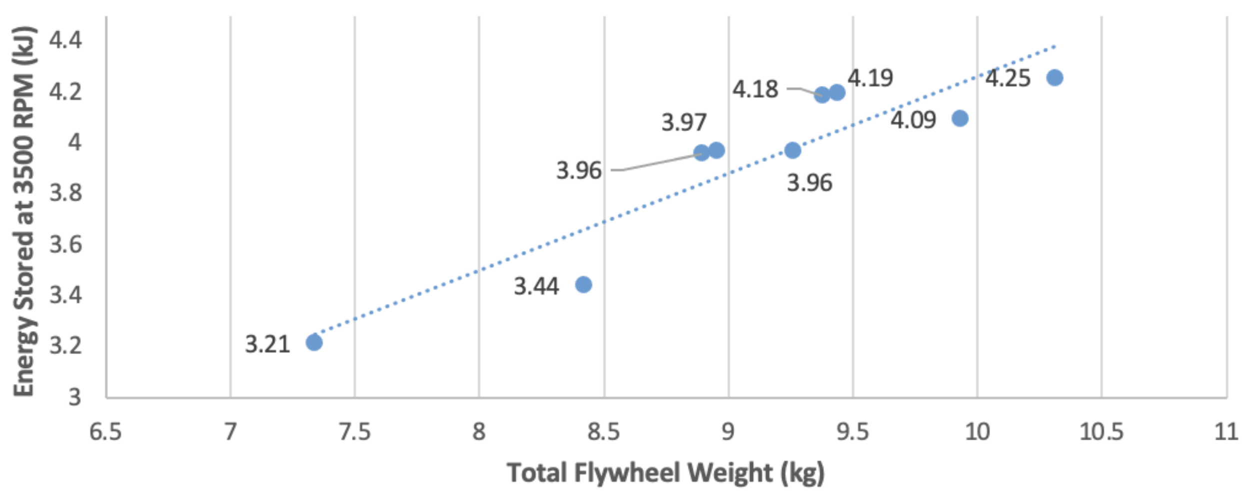


*Figure 2: Flywheel Dimension Trade Study*

Due to the large amount of energy involved in a heavy steel flywheel spinning at a high velocity, the team wanted to make sure the system had a high factor of safety and minimal deformation under load. FEA was performed on the flywheel at 4000 RPM and it was found to have a minimum factor of safety of 10.3 (Figure 3) and a maximum displacement of 4.9 µm (Figure 4).

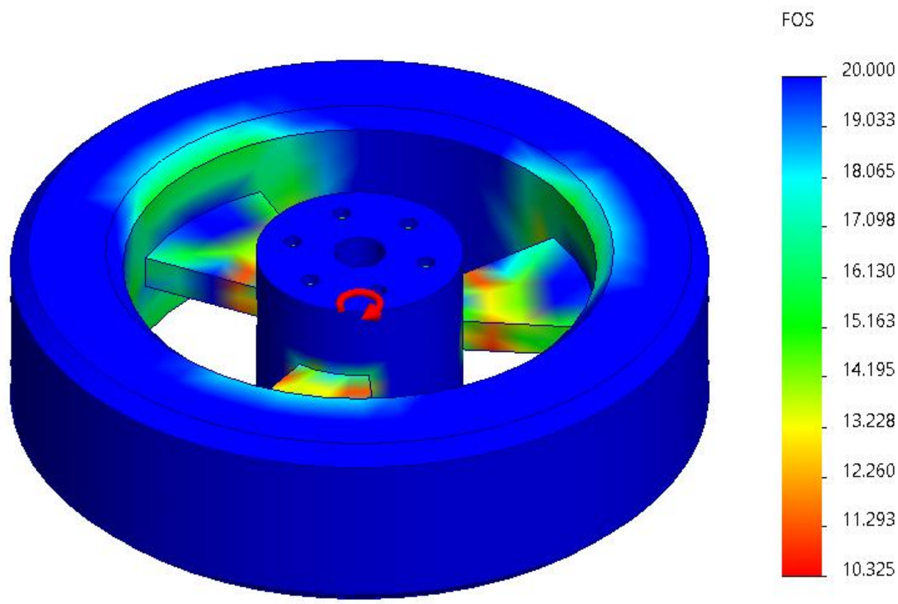


*Figure 3: Flywheel Factor of Safety Centrifugal Load Analysis*

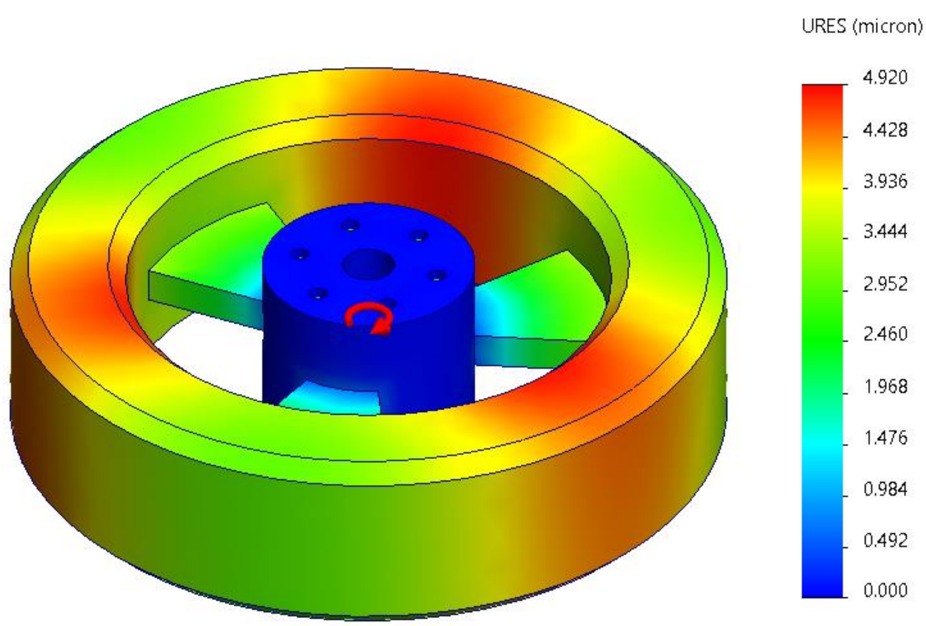


*Figure 4: Flywheel Centrifugal Load Displacement Analysis*

A vibrational analysis was also performed on the flywheel. The assembly was tested with a vibrational acceleration of 6 g's and a dampening ratio of 0.05 for steel structure. The maximum stress fluctuated between 0.15-3 MPa depending on the time interval of the test.

The time history graph shown in Figure 6 shows the response that the assembly had to the applied dynamic frequency. Initially, the system was excited by 6 g of vibrational acceleration in 0.01 s, but the vibration was quickly absorbed and dissipated by the natural dampening of the steel materials. The resonant frequency of the system was about 480 Hz in mode 2 during the test, which was in the circumstance of 6 g's of acceleration, which is not a common occurrence.

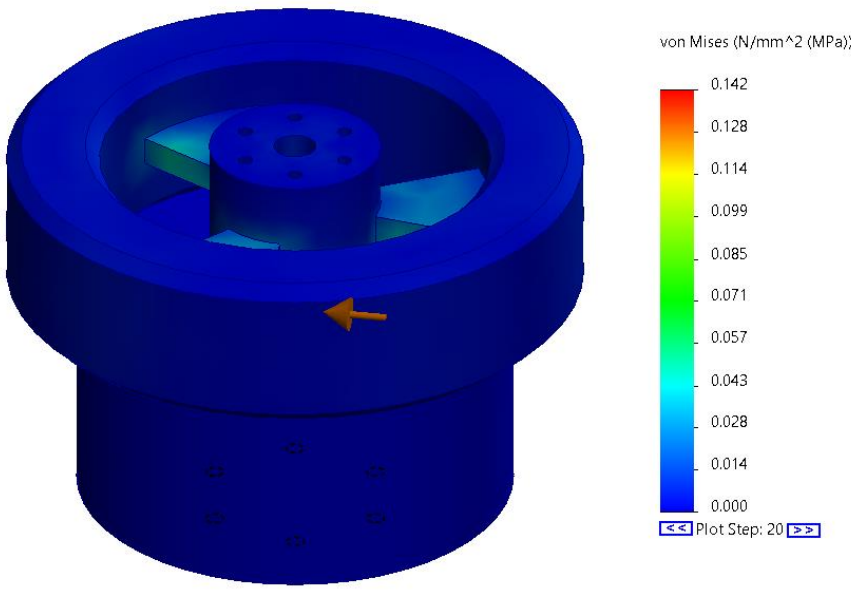


*Figure 5: Modal Stress Analysis of Flywheel with U15L Auxiliary Motor*

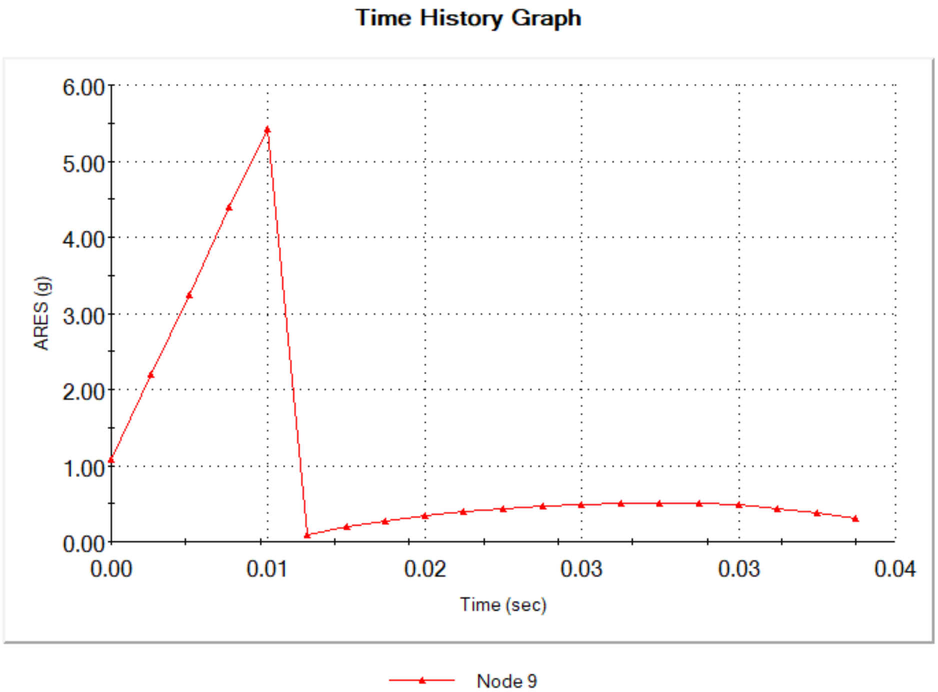


*Figure 6: Dynamic Frequency Response Graph*

## Section 3: Trailer Hitch Analysis

The hitch mounting system was designed using a kinematic study of the trailer to find the reaction forces under the maximum possible acceleration. This was done using the equation for force as a function of mass and acceleration (Equation 10), as well as a sum of moments about the rear axle (Equation 11). The moment about the rear axle due to rolling resistance is considered negligible. A lateral force is also accounted for; it is 1/3 the maximum force due to acceleration (to simulate the forces involved in evasive maneuvers). A deceleration of -49.1 $m/s^2$ (5 g) was chosen to verify the strength of the mount during emergency stops, such as sudden braking or a light impact. This deceleration is equivalent to the maximum deceleration of a Formula 1 racecar and is representative of a 10 kph impact with a solid object. This study allowed for an accurate analysis of the hitch brace to ensure its safety.

$$F_{accel} = m\alpha \tag{10}$$

$$N_1 b = Wa + F_{accel} d \tag{11}$$

*Table 8: Trailer Reaction Forces*

| Variables (Figure 16) | Value (Unit) |
|---|---|
| a | 0.165 m |
| b | 1.24 m |
| d | 0.230 m |

| | |
|---|---|
| Mass | 80 kg |
| Acceleration | -49.1 $m/s^2$ |
| Max Vertical Force ($N_1$) | 650 N |
| Max Compressive Force ($F_{accel}$) | 4,000 N |
| Max Lateral Force (1/3 of $F_{accel}$) | 1,333 N |

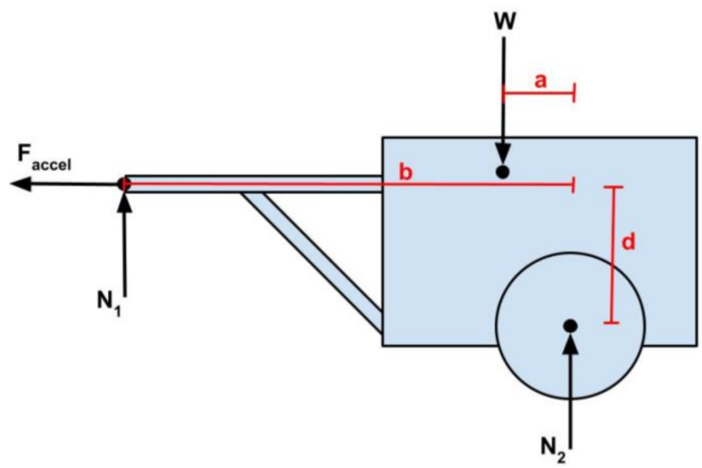


*Figure 7: Trailer Free Body Diagram*

A strain analysis was performed on the hitch using the maximum compressive force to ensure there would be no failure. A maximum strain of 2.8e-3 mm/mm was found.

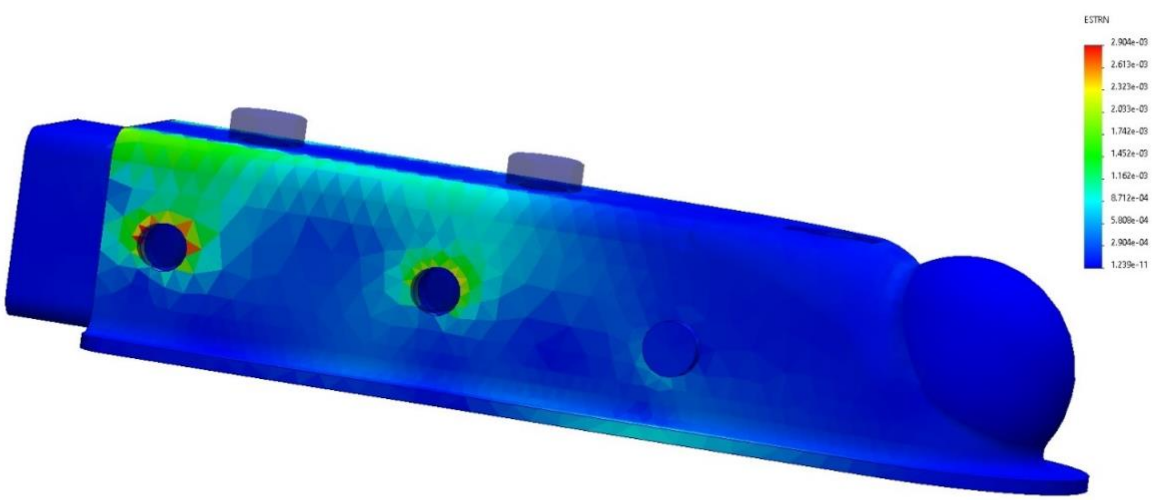


*Figure 8:Strain Testing On The Trailer Hitch*

## Section 4: Trailer CAD Models

The following CAD models were creating using models from the SDSU FSAE team. They were modified and added to in collaboration with Jack Muller from the All Brakes No Gas design team.

The following models (Figure 9 and 10) are the test bench with auxiliary motor and flywheel.

*Figure 9: Full Assembly Model View*

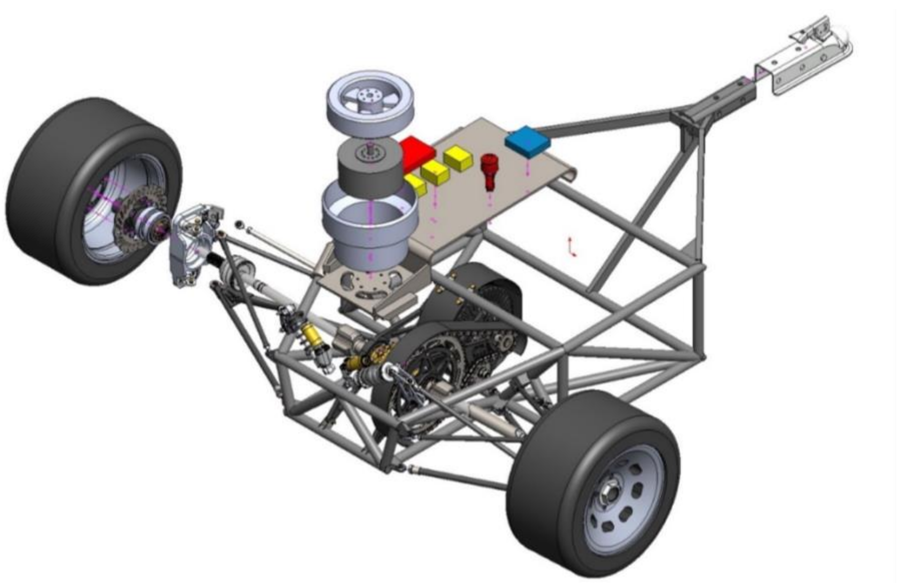

*Figure 10: Exploded View of the Full Assembly Model*

Figure 11 shows the original circuit mount alongside the auxiliary motor and flywheel and Figure 12 shows the new circuit mount following the system redesign. Figure 13 shows a load analysis of the mounting plate with a 20lb load. The maximum stress was abour 3.5 MPa, well below the yield stress of 460 MPa for 4130 steel. This mounting plate was later reduced in thickness to 1/8 in reduce weight and material cost.

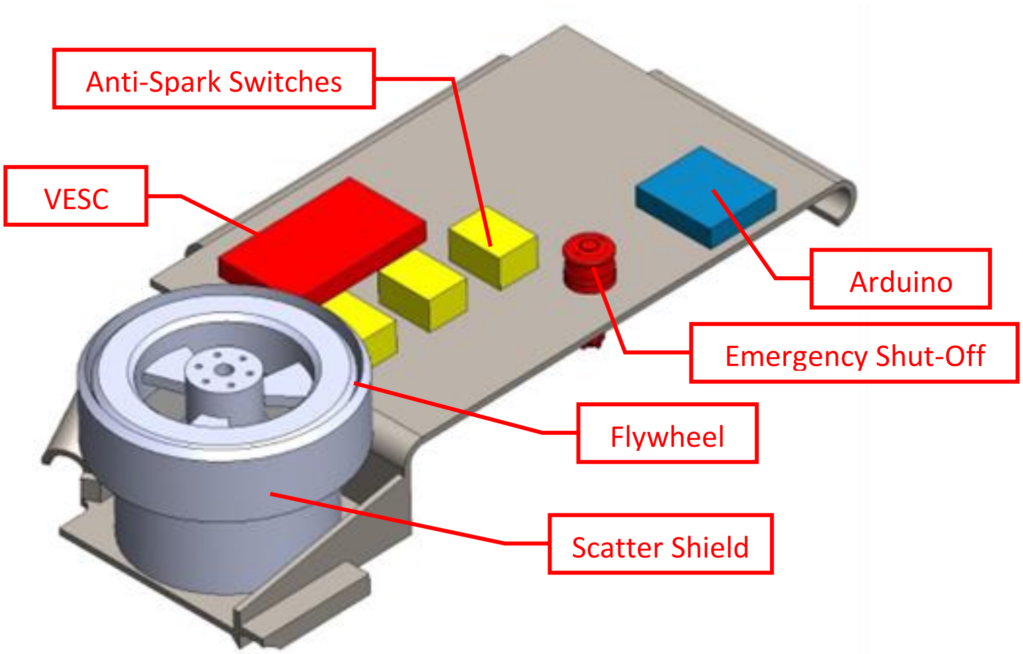


*Figure 11: Fall Semester Flywheel-Based Regenerative Braking System*

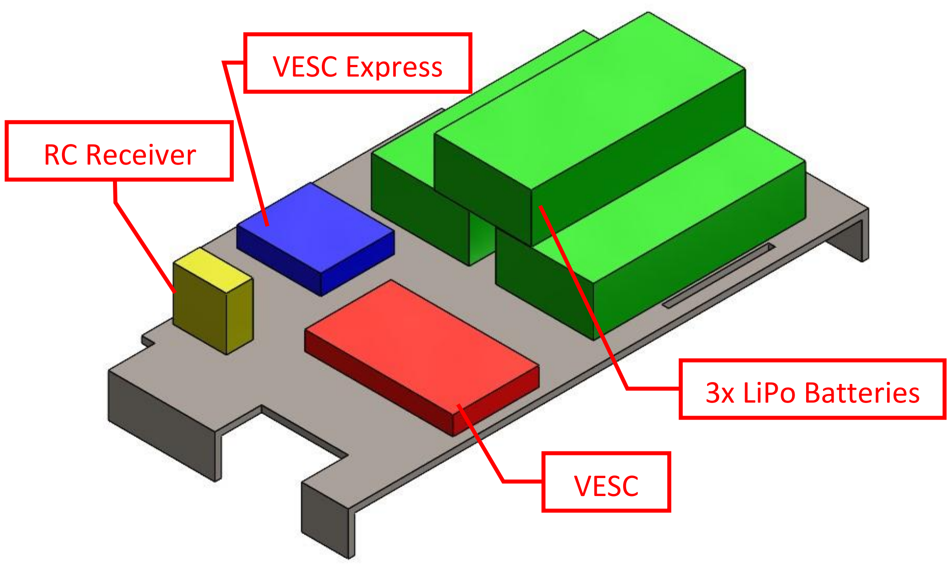


*Figure 12: Spring Semester Battery-Based Regenerative Braking System*

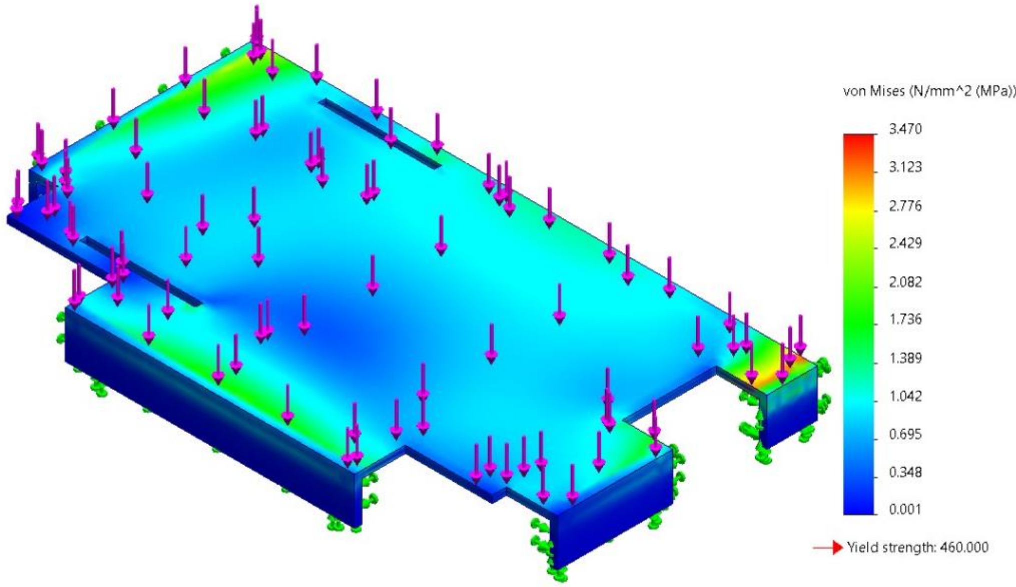


*Figure 13: Mounting Plate Stress Analysis Under 20 lbs Load*

Figure 14 shows the updated test bench model using the battery-based Regenerative Braking System

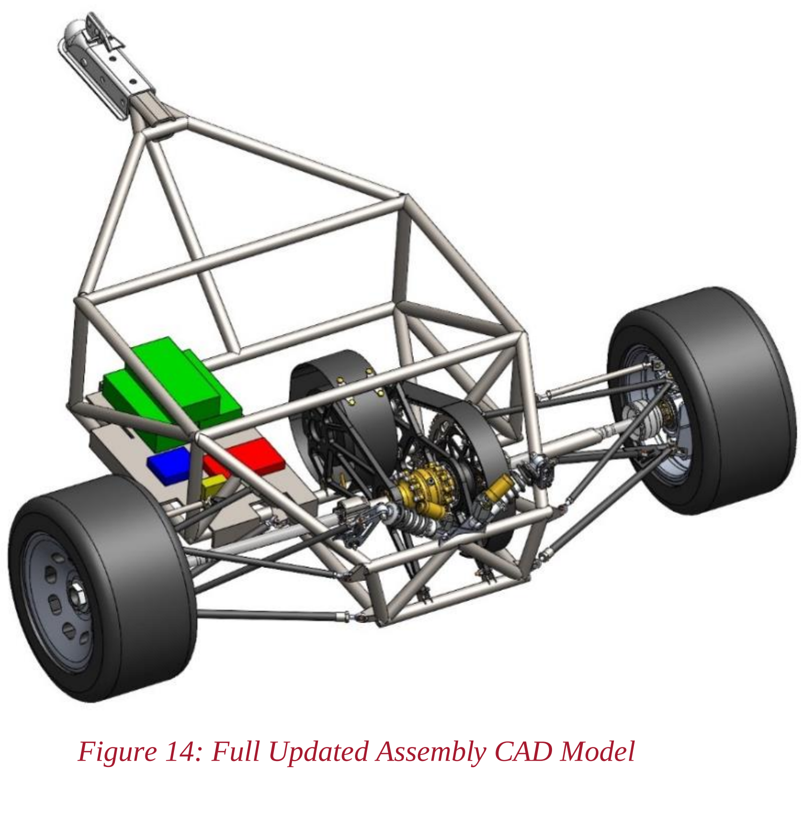

*Figure 14: Full Updated Assembly CAD Model*

## Section 5: Manufacturing and Assembly

The following section illustrates the manufacturing and assembly tasks performed by Henri Stephan for the All Brakes No Gas team. The main tube chassis structure along with other small CNC parts were outsourced due to lack of access to a welder, CNC, and significant workspace until the end of March.

*Table 9: Chassis Manufacturing*

| Part | Method |
| --- | --- |
| Suspension Tabs | **Waterjet** – Cut in SDSU machine shop using 1/16 in. steel sheet.<br>**TIG Welder** – Welded in EIS-106B.<br>**Hand Tools** – Some tabs had to be modified to ensure proper fitment and avoid potential interferences. |
| Waterproofing | **Hand Tools** – Sanded and Painted Chassis |
| Drivetrain/Scatter Shield Tabs | **Waterjet** – Cut in SDSU machine shop using 1/16 in. steel sheet. |
| Toe Links | **Abrasive Saw –** Shortened by 3/8 in.<br>**Hand Tools –** Sanded and painted. |

*Table 10: Drivetrain Unit Manufacturing*

| Part | Method |
| --- | --- |
| Idler Shaft | **CNC Lathe** – Cut and threaded in SDSU Aerospace machine shop.<br>**Sieg Mini Lathe** – Minor adjustments for proper fitment (lathe owned by Aztec Baja). |
| 65-Tooth Sprocket | **Waterjet** – Cut in SDSU machine shop using ¼ in. steel sheet. |
| Turnbuckles | **Sieg Mini Lathe** – Cut down and tapped with a 10-32 tap. Left-handed thread on one end and right-handed on the other. |
| Scatter-Shields | **Waterjet** – Tabs cut in SDSU machine shop using 1/16 in. steel sheet.<br>**Hand Tools** – Holes drilled, and minor adjustments made with angle grinder for fitment. |
| Mockup Pieces | **3D Printer** – Aztec Baja 3D printer for the idler shaft mockup as well as ZIP Launchpad resin printer for bearing mockups. This allowed the team to ensure the proper measurements for |

| | |
|---|---|
| | drivetrain alignment when welding drivetrain mount tabs. |

*Table 11: Circuit Mount Manufacturing*

| Part | Method |
|---|---|
| Mounting Plate | **Waterjet** – Cut in SDSU machine shop using 1/16 in. inch steel sheet.<br>**TIG Welder** – Welded in EIS-106B by the team.<br>**Hand Tools** – Holes were drilled to mount the housings; paint was applied for waterproofing. |

## Section 6: Manufacturing and Assembly Photos

The following photos illustrate some of the manufacturing and assembly process.

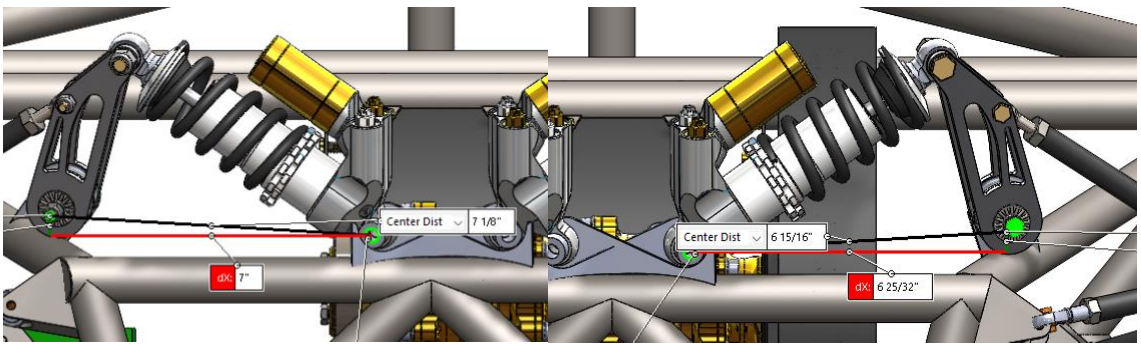

*Figure 15: Suspension Asymmetry, 5/32 in. Difference Between Left and Right*


*Figure 16: TIG Welded Suspension Tabs (top left, middle), Circuit Mount (top right), Scatter-Shields (bottom)*

*Figure 17: Machining Turnbuckles on Sieg Mini Lathe (left), Idler Shaft on CNC Lathe (right)*

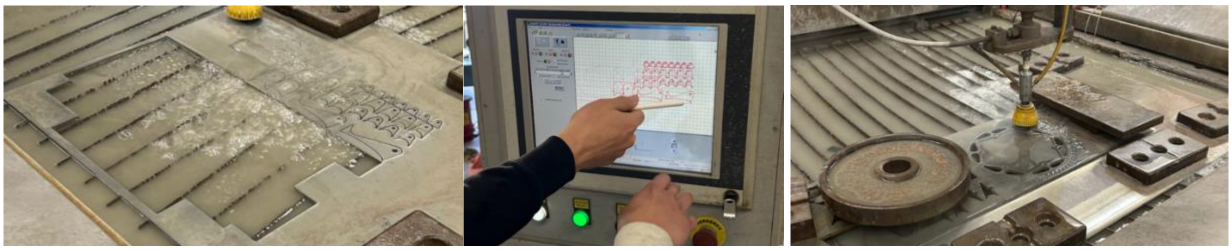

*Figure 18: Water-Jetting Tabs (left), Flow Path Software (middle), Water-Jetting 65-Tooth Sprocket (right)*

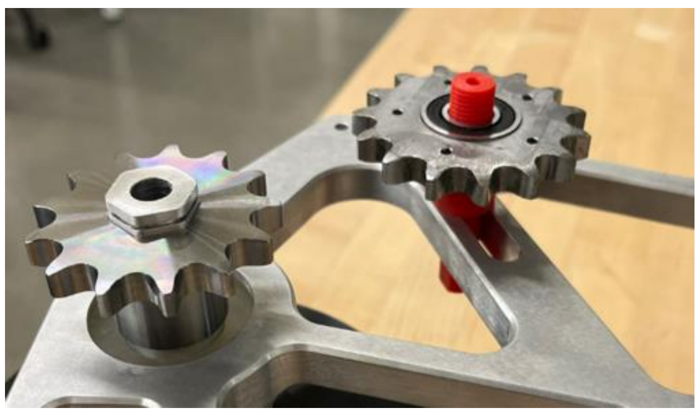

*Figure 19: 3D Printed Mockup Pieces in Place*

*Figure 20: Chassis Priming (left), Final Chassis Sealing (right)*

*Figure 21: Assembled Test Trailer (without axles, hubs, and wheels)*

## Section 7: Results and Presentation

The trailer was successfully assembled before the deadline and preliminary tests were performed to ensure proper function. The design was successfully presented during Senior Design Day and demonstrated for all those who were interested. The following image shows the team on design day and some of the data displayed during demonstrations. The Aztec Racing FSAE team is currently using the test bench to define efficiency of regenerative braking, refine their control system, and to draw in new members as a demonstration piece.

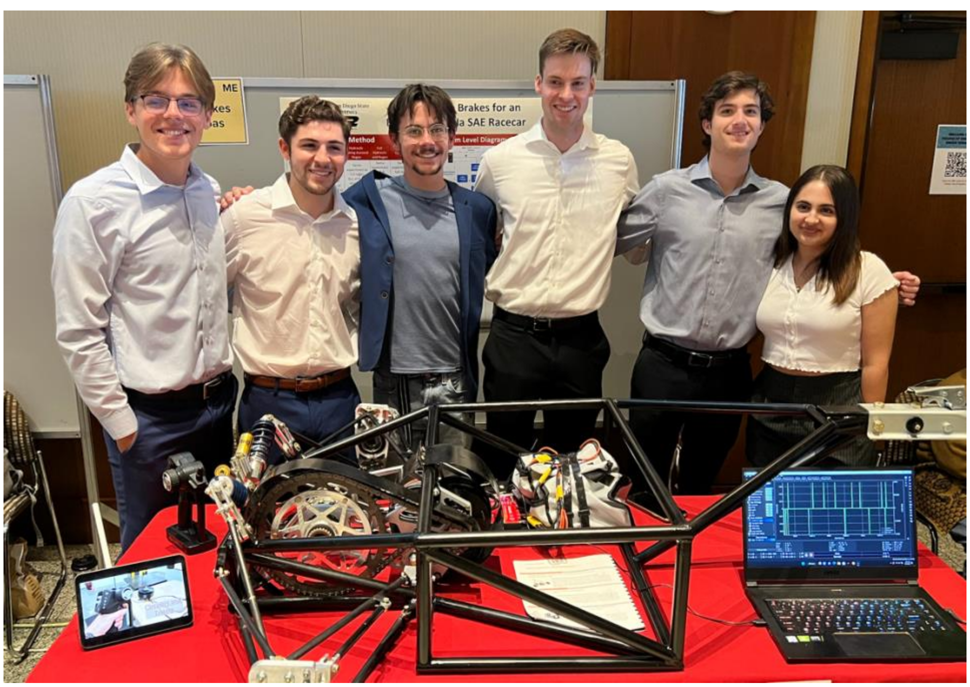

*Figure 22: All Brakes No Gas Team on Design Day*


*Figure 23: VESC Graphs*